

## Material properties

# Effect of carbonyl iron concentration and processing conditions on the structure and properties of the thermoplastic magnetorheological elastomer composites based on poly(styrene-*b*-ethylene-co-butylene-*b*-styrene) (SEBS)



Xiuying Qiao<sup>a,\*</sup>, Xiushou Lu<sup>a</sup>, Xinglong Gong<sup>b</sup>, Tao Yang<sup>c</sup>, Kang Sun<sup>a</sup>, Xiaodong Chen<sup>c</sup>

<sup>a</sup> State Key Laboratory of Metal Matrix Composites, Shanghai Jiao Tong University, Shanghai 200240, China

<sup>b</sup> CAS Key Laboratory of Mechanical Behavior and Design of Materials, Department of Modern Mechanics, University of Science and Technology of China, Hefei, Anhui 230027, China

<sup>c</sup> Shanghai Sunny New Technology Development Co., Ltd., Shanghai 201109, China

## ARTICLE INFO

## Article history:

Received 11 July 2015

Accepted 16 August 2015

Available online 20 August 2015

## Keywords:

Magnetorheological elastomer

SEBS

Carbonyl iron

## ABSTRACT

Isotropic and anisotropic thermoplastic magnetorheological elastomer (MRE) composites were prepared by melt blending carbonyl iron (CI) particles with poly(styrene-*b*-ethylene-co-butylene-*b*-styrene) (SEBS) matrix in the absence and presence of a magnetic field. Effects of CI concentration and processing conditions on the microstructure, thermal stability, mechanical properties, viscoelastic properties and magnetorheological properties of these MRE composites based on SEBS were investigated. Adding magnetic CI particles significantly improves the thermal stability and mechanical strength of SEBS matrix, but does not sacrifice the elasticity and toughness. The CI/SEBS composites, prepared with greater CI concentration at higher temperature, longer time and stronger magnetic field for pre-structuring, exhibit higher field induced modulus change and greater magnetorheological effect, due to the strengthening of mutual particle interactions and the formation of longer and more ordered chain structures.

© 2015 Elsevier Ltd. All rights reserved.

## 1. Introduction

Magnetorheological elastomers (MRE) are a type of novel smart material that exhibit rapidly and reversibly controllable mechanical properties under the action of an external magnetic field, due to the interaction of micrometer-sized magnetically permeable particles in the non-magnetic matrix [1]. In general, the MRE materials can be classified into two categories, isotropic and anisotropic MREs prepared without and with external magnetic field. The magnetizable particles are dispersed uniformly and randomly in the former MREs and form ordered chain or column structures oriented in the magnetic field direction in the latter MREs. Besides the superior magnetorheological effect (MR effect), MRE has been demonstrated to possess other special properties such as electrical resistance, piezoresistivity, thermoresistance, magnetoresistance and magnetostriction [2–5]. These particular features make MRE

attract much attention and gain broad application prospects in the fields of adaptive tuned vibration absorbers and mass dampers, sensors and actuators [6–8].

In general, degree of freedom of the magnetic particle movement is governed by the elastomer matrix, and the MR effect is usually small in a hard matrix as compared to a soft matrix. Silicon rubber is commonly chosen to fabricate MRE composites because of its softness allowing easier movement and good dispersion of magnetic particles in liquid precursors during synthesis. However, the mechanical properties of silicon rubber cannot satisfy some application requirements due to its low stiffness [9], and great efforts have been made to further improve the performance of MRE by using other rubbers such as natural rubber [9], polyurethane (PU) [10–12], isobutylene–isoprene [13], cis-polybutadiene [14] and rubber blends [15,16]. In this study, styrenic thermoplastic elastomer (TPE) was chosen as the MRE matrix due to its good mechanical properties as well as good recyclability and processability [17]. As for the magnetizable particles, carbonyl iron (CI) [18], Fe<sub>3</sub>O<sub>4</sub> [19], Fe nanowires [20], nickel [5] and hybrid fillers [21] have been utilized, of which CI particles have been most commonly

\* Corresponding author.

E-mail address: [xyqiao@sjtu.edu.cn](mailto:xyqiao@sjtu.edu.cn) (X. Qiao).

used because of, not only their excellent magnetic properties, but also their spherical shape that helps MRE applications. The chemical features, size and shape of the magnetizable particles obviously influence and govern the MRE properties [18]. Under the action of an external magnetic field, the field induced interactions between the magnetizable particles can lead to a change in the particle preconfiguration from isotropic random dispersion to anisotropic ordered chains or complex three dimensional structures. There are also several methods to improve the MR effect of MRE materials, including choosing softer rubber matrix [22], adding plasticizer to soften the matrix [23], introducing compatibilizer to enhance the interactions between filler and matrix [24] and surface treatment of CI particles by polymer coating or surfactant modification [10,25,26].

In this paper, we prepared isotropic and anisotropic thermo-plastic MRE composites with a tri-block polymer poly(styrene-*b*-ethylene-co-butylene-*b*-styrene) (SEBS) as matrix and silane coupling agent modified CI particles as magnetic particles. The effects of CI concentration and processing conditions on the micro-structure, thermal stability, mechanical properties, viscoelastic properties and magnetorheological properties of these CI/SEBS composites were investigated. SEBS has no C=C double bonds in the EB block and exhibits good thermal stability and is relatively climate proof (against UV/Ozone). SEBS plasticized by white oil is very soft and SEBS based MRE is expected to show a high MR effect. Meanwhile, the usage of surface-modified CI particles helps to improve the MR effect of CI/SEBS composites due to the enhancement of interfacial compatibility, which has been verified in our previous work [27].

## 2. Experimental

### 2.1. Materials

Poly(styrene-*b*-ethylene-co-butylene-*b*-styrene) (SEBS) powder (Taiplo-SEBS-3151) was purchased from TSRC Corporation (China) and utilized as received. Its molecular characteristics are  $M_w = 2.7 \times 10^5$ ,  $M_w/M_n = 1.06$ , and S content  $w_s = 32$  wt%. White oil suited for softening/processing SEBS TPEs, was purchased from Shanghai Daliang Chemical Co. Ltd. (China) and utilized as received. This oil is a purified mixture of different saturated hydrocarbon molecules dissolving EB blocks but precipitating S blocks. The SEBS matrix utilized for preparing MRE composites is a SEBS/oil 1/2 wt/wt mixture and contains glassy, spherical S domains (at room temperature) that serve as physical crosslinks at low  $T$ . The EB mid-blocks form a rubbery, continuous phase swollen with the white oil.

Commercially available carbonyl iron (CI) particles (FTF-1; Jianyou Hebao Nanomaterial Co. Ltd., China) were utilized as received. These CI particles have an average particle diameter of 3.5  $\mu\text{m}$ , Fe content of ~98.3% and particle density of 7.64 g/cm<sup>3</sup>. The CI particles are spherical and have a relatively smooth surface, as noted from the Scanning Electron Microscope (SEM) image. (3-Aminopropyl) triethoxysilane (KH550, C<sub>9</sub>H<sub>23</sub>NO<sub>3</sub>Si), purchased from Jinzhou Jiangnan Fine Chemical Co. Ltd. (China), was used for modifying the CI particle surface to enhance the affinity between the CI particles and SEBS matrix.

### 2.2. MRE preparation

Table 1 summarizes the composition of SEBS matrix and CI/SEBS composites. The SEBS matrix contains 33.3 wt% SEBS and 66.7 wt% white oil. The 40CI-SEBS and 70CI-SEBS composites are mixtures of CI particles in this SEBS/oil matrix with CI concentrations of 40 and 70 wt%, respectively. CI particles were modified by silane coupling agent at a concentration of 2 wt% to the CI particle mass before

**Table 1**  
Composition of the SEBS matrix and CI/SEBS composites.

Sample code	SEBS (wt%)	White oil (wt%)	Carbonyl iron (wt%)
SEBS*	33.3	66.7	0
40CI-SEBS	20	40	40
70CI-SEBS	10	20	70

Note: \*SEBS matrix containing white oil.

mixing with the SEBS matrix.

The CI particles were pretreated with the silane coupling agent in a blender for 3 min at a low mixing speed and then for 8 min at a high mixing speed at room temperature. SEBS powders were mixed with the white oil in a blender for about 10 min at a low speed to allow SEBS to fully absorb the oil. The starting compounds for the CI/SEBS composite preparation were obtained by mixing prescribed masses of this SEBS matrix and the silane coupling agent modified CI particles at high speed for 10 min at room temperature. The compound thus obtained was extruded at 220 °C in a co-rotating twin screw extruder with a screw L/D ratio of 25:1 and a screw speed of 30 rpm, cooled in a cold water bath, stretched during haul-off, pelletized to granules, and then dried at 80 °C for 3 h before molding. For preparation of the isotropic MRE, the CI/SEBS composite granules were molded into films of 2 mm thickness at 160 °C (or higher  $T$ ) for 10 min in an ordinary press in the absence of external magnetic field. On the other hand, for preparation of the anisotropic MRE, the CI/SEBS composite granules were molded into sheets of 3 mm thickness at 160 °C for 20 min in a home-made magnet-heat coupled device under a magnetic field with intensity ranging from 0 to 1200 mT. During this fabrication process, the nominal magnetic field intensity was set with a current controller and the actual intensity was measured with a Teslometer (Shanghai Hengtong Magnetolectricity Co. Ltd, China). The anisotropic composites thus obtained were designated as  $n$ CI-SEBS- $m$ , where  $n$  represents the CI concentration (in wt%) and  $m$  represents the magnetic field intensity (in mT) used during fabrication.

### 2.3. Morphology observation

The morphology of isotropic and anisotropic CI/SEBS composites was observed with a S-2150 Scanning Electron Microscope (SEM; Hitachi, Japan) operated at an accelerating voltage of 20 KV. Before SEM observation, the CI/SEBS composite samples pretreated with liquid nitrogen and freeze-fractured were coated with a thin gold layer to avoid the surface charging.

### 2.4. Thermal stability

With the use of a TGA2050 Thermogravimetric Analyzer (TA, USA), the weight change of the CI/SEBS composites was examined from room temperature to 800 °C at a heating rate of 10 °C/min in a nitrogen atmosphere.

### 2.5. Mechanical properties

The tensile tests were performed on a CMT6104 Universal Tensile Tester (Sans Testing Machine, China) according to GB/T 528-1998 standard at room temperature. The dumbbell-shaped specimens were stretched at a crosshead rate of 500 mm/min until rupture. Five specimens for each sample were tested to obtain the average value.

### 2.6. Linear viscoelasticity analysis

For basic characterization of the SEBS matrix and CI/SEBS

composites, linear viscoelastic measurements were conducted at 20 °C in the absence of magnetic field with a stress-controlled rheometer (HAAKE MARS II, Thermo Electron, Germany). To ensure the linear viscoelastic regime, a dynamic strain sweep was conducted in a range of  $\gamma_0 = 0.00001$ –1 (0.001%–100%) at a frequency of  $\omega = 1$  rad/s. Dynamic frequency sweeps were performed from 100 rad/s to 0.1 rad/s with a strain of 0.03% in the linear regime.

### 2.7. Magnetic dynamic mechanical analysis (MDMA)

The magnetorheological (MR) properties of the CI/SEBS composites were examined through a modified Triton 2000B Dynamic Mechanical Analysis (Triton Technology, UK) system equipped with a home-made electromagnet that could generate a magnetic field of various intensities. This modified DMA system is referred to as MDMA, and the dimensions of the sample specimen for tests were 10 mm × 10 mm × 3 mm (length, width and thickness). The measurements were made at a frequency of 1 Hz, strain amplitude of 0.0667% and room temperature under the magnetic field to record the field induced dynamic shear modulus response. The direction of the external magnetic field was perpendicular to the surface of tested sample. This direction was parallel to the chain structure of the CI particles in the anisotropic CI/SEBS composites, so that the modulus measured under the magnetic field detected the response of the composites in the direction perpendicular to those chains.

## 3. Results and discussion

### 3.1. Morphology observation

Fig. 1 illustrates the SEM images of the isotropic and anisotropic CI/SEBS composites prepared in the absence and in the presence of

a magnetic field. It can be found from Fig. 1 that, in the isotropic CI/SEBS composites (Fig. 1(a) and (b)), the spherical silane coupling agent modified CI particles (white dots) are uniformly and randomly dispersed in the SEBS matrix without forming large aggregates. In fact, CI particles are very different from the SEBS matrix chemically, and this good dispersion of CI particles in the SEBS matrix may imply that adsorbed layer should exist and this adsorbed layer can effectively increase the particle volume fraction. However, in the anisotropic CI/SEBS composites (Fig. 1(c) and (d)), the CI particles form chain-like structures aligned in the direction of magnetic field that was loaded during composite fabrication, due to the mutual attractions between these magnetizable particles. Obviously, during the preparation of anisotropic composite, when the SEBS matrix lost its elasticity at high temperature above 160 °C, the CI particles were reorganized from the random dispersion into ordered orientated distribution in the soft liquid SEBS matrix under the action of the magnetic field. It can also be observed from Fig. 1 that, before magnetic saturation, the particle chain length and orientation degree of CI particles in the CI/SEBS composites increase with enhancement of magnetic field intensity. Actually, the state of CI particle distribution in MRE matrix will strongly influence the MR effect of MRE composites, and longer particle chains and higher orientation degree of CI particles will make MRE composites present higher MR effect and stronger smart magnetic response, showing greater modulus changes with the magnetic field. This will be verified by the MDMA results in Section 3.5.

### 3.2. Thermal stability

The TGA and DTG curves of the SEBS matrix and CI/SEBS composites are given in Fig. 2 to confirm the effect of CI filling on the thermal stability of SEBS matrix. The thermal stability parameters of 10% weight loss temperature ( $T_{10wt\%}$ ), peak decomposition temperature ( $T_p$ ), peak decomposition rate ( $R_p$ ) and residue during

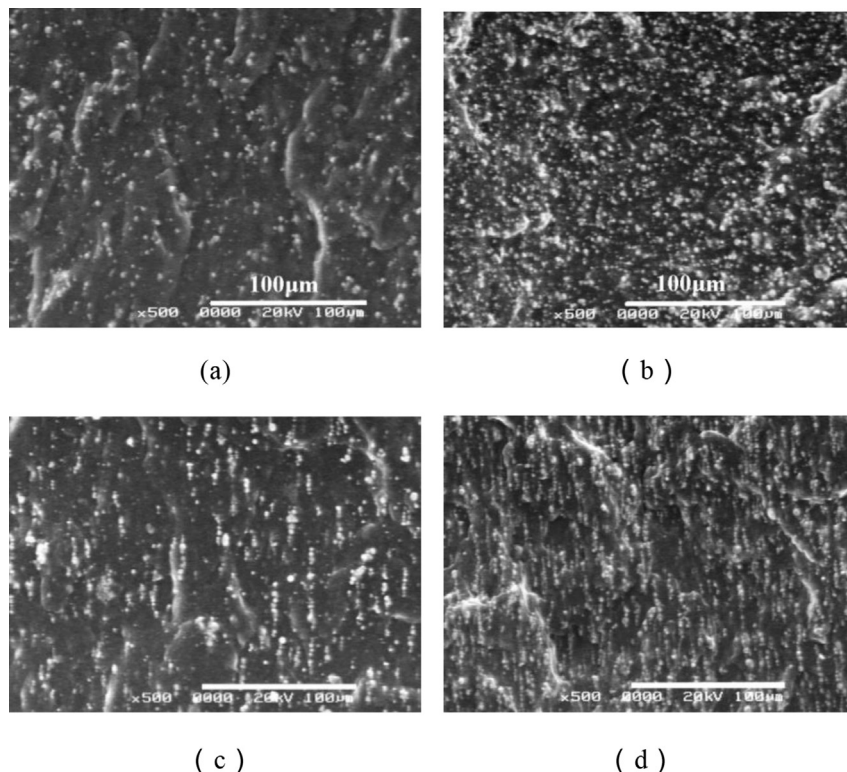


Fig. 1. SEM images of the isotropic and anisotropic CI/SEBS composites: (a) 40CI-SEBS; (b) 70CI-SEBS; (c) 40CI-SEBS-900mT; (d) 70CI-SEBS-900mT. The bar scale is 100 μm.

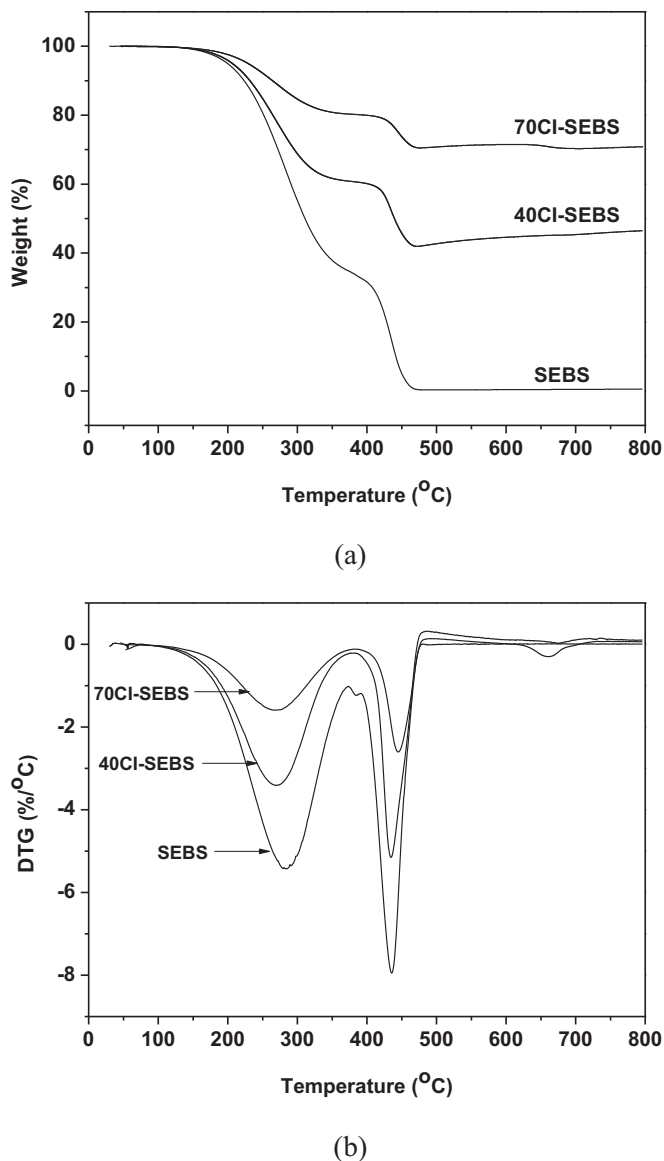


Fig. 2. Thermogravimetric analysis results of the isotropic CI/SEBS composites: (a) TGA curves; (b) DTG curves.

the thermal decomposition process obtained from the TGA and DTG results are listed in Table 2. Both SEBS matrix and CI/SEBS composites exhibit two degradation processes, which can be attributed to the degradation of plasticizer oil in a low temperature region, with maximum degradation at 283.6 °C, and SEBS at high temperature region, with maximum degradation at 435.6 °C [28]. Obviously, the addition of CI particles notably improves the thermal stability of SEBS matrix with the obvious increase of both  $T_{10wt\%}$  and  $T_{P2}$  and decrease of  $R_P$ . Moreover, the addition of CI particles makes  $T_{P1}$  shift to lower temperature but  $T_{P2}$  shifts to higher temperature, exhibiting different influences on the degradation of white oil and

SEBS molecules. Just as mentioned in our previous work [27], there should be an interface between CI particles and styrenic thermoplastic elastomer, and the modification of coupling agent on the CI particle surface will improve the interfacial compatibility between the particle and matrix. The remarkable interactions between SEBS molecules and CI particles due to the adsorption of SEBS matrix layers on the polar CI particle surface reduce the degradation at a certain temperature and maximum degradation rate of SEBS molecules. After filling with CI particles, although the peak degradation temperature of plasticization oil is decreased by more than 10 °C, the maximum degradation rate of this oil is still decreased significantly.

### 3.3. Mechanical properties

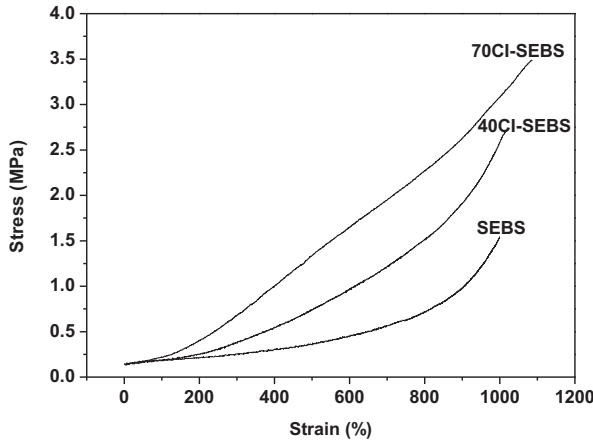
The mechanical properties of the composites are closely related to filler dispersion. The stress–strain curves of the SEBS matrix and CI/SEBS composites and the obtained mechanical property parameters of tensile strength and elongation at break are shown in Fig. 3. During the tensile test, both SEBS and CI/SEBS composites exhibit superior elastic behavior, without any breakage even when the measured strain exceeds 1000%. It should be noted that, although large amounts of CI particles (70wt%) are filled into the elastomer matrix, the typical elastomer behavior and toughness of the SEBS matrix are not obviously influenced, and the elongation at break of 70CI-SEBS composite still exceeds 1000%. Thus, it can be seen that good interfacial compatibility exists between the surface modified CI particles and SEBS matrix, and the CI/SEBS composites show excellent softness similar to the SEBS matrix due to the weak influence of the interfacial layer thickness. Moreover, the tensile strength of SEBS matrix is also improved after CI addition, more than doubled at CI concentration of 70wt%.

### 3.4. Linear viscoelasticity

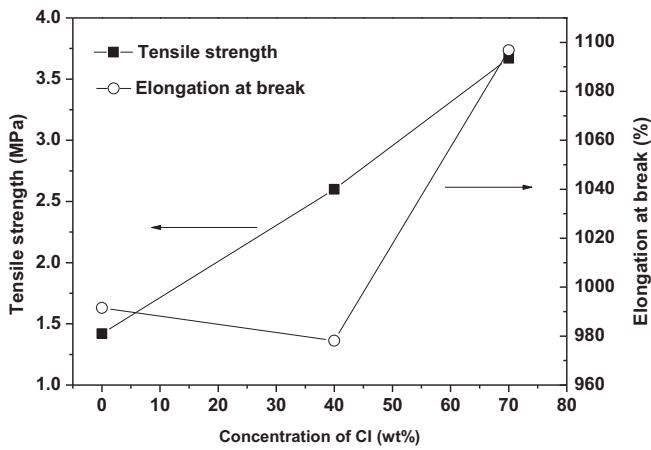
Fig. 4 shows the angular frequency ( $\omega$ ) dependence of the storage modulus  $G'$  measured for the isotropic and anisotropic CI/SEBS composites at 20 °C in the absence of the magnetic field. For comparison,  $G'$  data of the SEBS matrix is also shown. The shear strain amplitude was kept small (0.03%) to ensure the linearity of the data. For all these materials, the loss modulus  $G''$  (not shown here) was much smaller than  $G'$  at all frequencies, indicating the remarkable elastic-like behavior of the SEBS matrix and CI/SEBS composites. The elastic plateau of  $G'$  exhibited by SEBS matrix can be attributed to the entanglement network of the middle EB blocks swollen with the white oil (EB-selective solvent), and physically cross-linked by the spherical domains of the end-S blocks. The SEBS matrix contains 67 wt% of the EB-selective white oil (cf. Table 1) and, therefore, forces the S blocks (of a small volume fraction  $\phi_S = 0.086$ ) to form spherical domains. The weak  $\omega$  dependence of  $G'$  data of the CI/SEBS composite is similar to that of the SEBS matrix, but the  $G'$  value increases with increase of CI particle concentration and magnetic field intensity used during composite fabrication. This behavior suggests that the uniformly dispersed CI particles behave as simple fillers, and the CI particle chains formed during anisotropic composite fabrication further strengthen the

Table 2  
The thermal parameters of 10wt% loss temperature ( $T_{10wt\%}$ ), peak decomposition temperature ( $T_P$ ), peak decomposition rate ( $R_P$ ) and residue during the thermal decomposition process of the isotropic CI/SEBS composites obtained from the thermogravimetric analysis results.

Sample code	$T_{10wt\%}$ (°C)	$T_{P1}$ (°C)	$T_{P2}$ (°C)	$R_{P1}$ (%/°C)	$R_{P2}$ (%/°C)	Residue (%)
SEBS	223.5	283.6	435.6	5.4	7.9	0.5
40CI-SEBS	231.7	270.1	435.8	3.4	5.1	46.5
70CI-SEBS	264.2	269.5	444.8	1.6	2.6	70.9



(a)



(b)

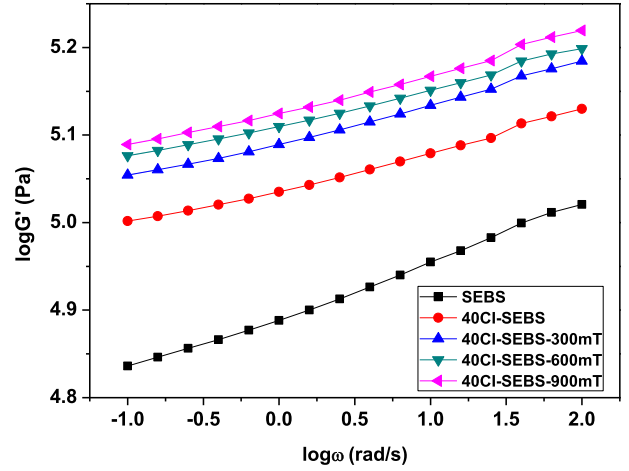
Fig. 3. Tensile test results of the isotropic CI/SEBS composites: (a) strain-stress curves; (b) tensile strength and elongation at break.

modulus of the composites as fiber reinforcement agent.

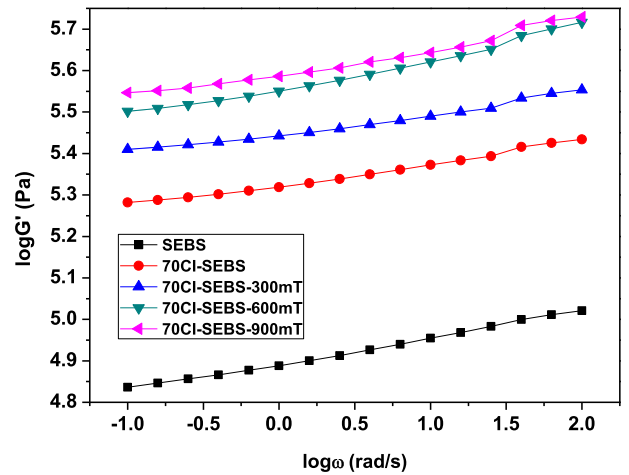
### 3.5. Magnetorheology properties

#### 3.5.1. Effect of pre-structure temperature and time

Fig. 5 illustrates the plots of shear storage modulus against magnetic field intensity obtained from MDMA measurements for the anisotropic 70CI-SEBS-600mT composites fabricated at the same magnetic field intensity ( $\psi_{pre}$ ) but different temperature ( $T_{pre}$ ) and time ( $t_{pre}$ ). It can be observed from Fig. 5 that the storage modulus  $G'$  exhibits similar change tendency under the magnetic field for all the composites, increasing rapidly with increasing field intensity  $\psi$  up to a threshold value of  $\psi_c \cong 600\text{--}700\text{ mT}$ , and then leveling off to a steady value  $G_{M,E}'$ . The equilibrium storage modulus  $G_{M,E}'$  is larger for the composite pre-structured at higher  $T_{pre}$  for the same period of 15 min and the composite pre-structured for longer  $t_{pre}$  at a given  $T_{pre}$  ( $160^\circ\text{C}$ ). However,  $G_{M,E}'$  becomes independent of  $t_{pre}$  for sufficiently long times ( $t_{pre} \geq 20\text{ min}$ ), and high  $T_{pre}$  and long  $t_{pre}$  during the pre-structure process have equivalent effect on  $G_{M,E}'$ , which can be verified by the overlapping of the curves of the composites prepared at  $160^\circ\text{C}$  for 20 and 30 min, and the approaching of the curves of the composites prepared at  $160^\circ\text{C}$  for 30 min and  $180^\circ\text{C}$  for 15 min. These results reveal that  $G_{M,E}'$  is governed by the chain structure of the CI particles in anisotropic CI/



(a)



(b)

Fig. 4. Double-logarithmic plots of storage modulus versus frequency of the SEBS matrix and the isotropic and anisotropic CI/SEBS composites measured in the absence of magnetic field: (a) 40CI-SEBS composites; (b) 70CI-SEBS composites.

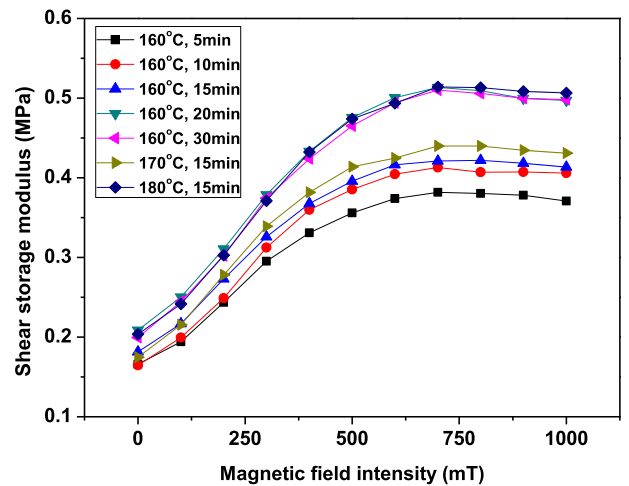


Fig. 5. Plots of shear storage modulus against magnetic field intensity obtained from MDMA measurements for the anisotropic 70CI-SEBS-600mT composites fabricated at the same magnetic field intensity but different temperature and time.

SEBS composites. Higher  $T_{pre}$  allows the CI particles to move more easily in the softer SEBS matrix, and longer  $t_{pre}$  allows larger displacement of the CI particles, both resulting in the formation of longer and more ordered chain structures. The  $t_{pre}$  independence of  $G_{M,E'}$  may reflect the equilibration of the particle position in the chain structure. Thus, it can be seen that the magnetorheological properties of the CI/SEBS composites can be well controlled by the pre-structure temperature and time, and the MR performance of MRE composites can be easily tuned by the processing conditions to a designated level during anisotropic composite fabrication.

One of the most important parameters describing the MR effect of MRE is the shear modulus change caused by the magnetic field. The shear storage modulus and MR effect of the anisotropic 70CI-SEBS-600mT composites obtained from Fig. 5 are listed in Table 3, in which  $G_0'$  is initial storage modulus without external magnetic field,  $G_{M,E'}$  is equilibrium storage modulus under saturated magnetic field,  $\Delta G'$  is the value of  $G_{M,E'}$  subtracting  $G_0'$  corresponding to the absolute MR effect, and  $\Delta G'/G_0'$  is the relative MR effect. It can be seen from Table 3 that  $G_0'$  shows the same change tendency with  $T_{pre}$  and  $t_{pre}$  as  $G_{M,E'}$  does, but the absolute and relative MR effect exhibits a little fluctuation with the changes of  $T_{pre}$  and  $t_{pre}$  due to increase of both  $G_0'$  and  $G_{M,E'}$  with  $T_{pre}$  rising and  $t_{pre}$  lengthening. However, the MR effect still reaches a maximum value for the CI/SEBS composite pre-structured at higher  $T_{pre}$  and longer  $t_{pre}$ , 180 °C for 15 min and 160 °C for 30 min.

### 3.5.2. Effect of pre-structure magnetic field intensity and CI concentration

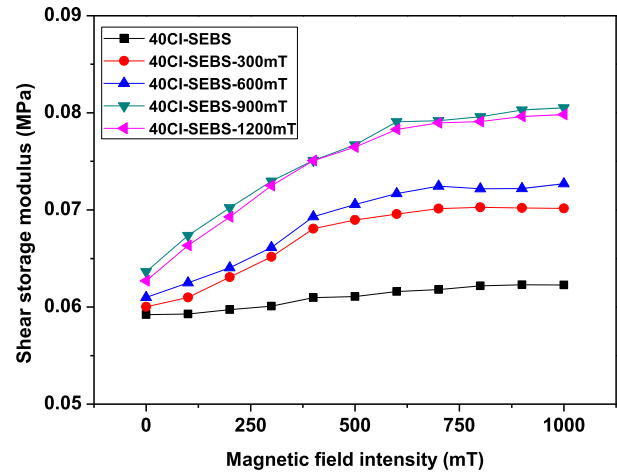
Fig. 6 gives the plots of shear storage modulus against magnetic field intensity obtained from MDMA measurements for the isotropic and anisotropic CI/SEBS composites, in which the anisotropic composites were pre-structured at 160 °C for 20 min. The magnetorheological property parameters of  $G_0'$ ,  $G_{M,E'}$ ,  $\Delta G'$  and  $\Delta G'/G_0'$  obtained from Fig. 6 are listed in Table 4. In Fig. 6, similar to the results of the natural rubber [29], silicon rubber [30] and PU [23] based MRE, the shear storage modulus of both isotropic and anisotropic CI/SEBS composites increases with the external magnetic field intensity  $\psi$  before reaching magnetic saturation, which agrees well with the theoretical analysis based on the field-induced dipole magnetic forces between the particles. The storage modulus of  $G_0'$  and  $G_{M,E'}$  and MR effects of  $\Delta G'$  and  $\Delta G'/G_0'$  of the CI/SEBS composites are remarkably increased with the increase of CI particle concentration and  $\psi_{pre}$  used for anisotropic composite preparation. On the one hand, the effect of CI particle concentration on the magnetorheological property is much greater for the anisotropic composites than for the isotropic composites. On the other hand,  $\psi_{pre}$  merely shows obvious influence on the magnetorheological properties of the composites before attaining magnetic

**Table 3**

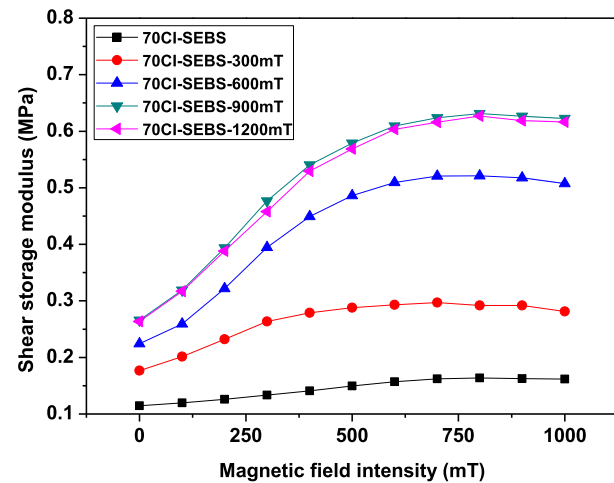
Shear storage modulus and MR effect of the anisotropic 70CI-SEBS-600mT composites fabricated at the same magnetic field intensity but different temperature and time obtained from the MDMA measurements.

Temperature and time	$G_0'$ (MPa)	$G_{M,E'}$ (MPa)	$\Delta G'$ (MPa)	$\Delta G'/G_0'$ (%)
160 °C, 5 min	0.166	0.382	0.216	130.1%
160 °C, 10 min	0.165	0.413	0.248	150.3%
160 °C, 15 min	0.182	0.421	0.239	131.3%
160 °C, 20 min	0.209	0.514	0.305	145.9%
160 °C, 30 min	0.199	0.510	0.311	156.3%
170 °C, 15 min	0.175	0.440	0.265	151.4%
180 °C, 15 min	0.204	0.514	0.310	152.0%

Note:  $G_0'$  is initial storage modulus without external magnetic field.  $G_{M,E'}$  is equilibrium storage modulus under saturated magnetic field.  $\Delta G'$  is the value of  $G_{M,E'}$  subtracting  $G_0'$ , corresponding to the absolute MR effect.  $\Delta G'/G_0'$  is the relative MR effect.



(a)



(b)

**Fig. 6.** Plots of shear storage modulus against magnetic field intensity obtained from MDMA measurements for the isotropic and anisotropic CI/SEBS composites: (a) 40CI-SEBS composites; (b) 70CI-SEBS composites.

saturation, the same as  $\psi$  does during MDMA measurements. In the isotropic CI/SEBS composites, the CI particles disperse randomly and uniformly, while in the anisotropic composite the CI particles are reorganized into chain-like structures aligned in the magnetic field direction, and this alignment is enhanced and particle chains become longer when higher  $\psi_{pre}$  is operated. Clearly, increasing magnetic particle amount and  $\psi_{pre}$  helps to strengthen the mutual particle interactions and enhance the degree of alignment and orientation of CI particles, thus making the magnetic particles possess more ordered and longer chain structures. Therefore, the  $n$ CI-SEBS- $m$  composites with larger  $n$  and  $m$  exhibit higher magnetorheological properties. However, higher  $\psi_{pre}$  also elevates the initial storage modulus of the composites, and the relative MR effect of the anisotropic 70CI-SEBS composites prepared at 900 mT and 1200 mT is a little lower than that of the 70CI-SEBS composite prepared at 600 mT.

It was found that the magnetically induced modulus  $G_M(\psi)$  is proportional to the square of the magnetic field intensity  $\psi$  ( $G_M(\psi) \propto \psi^2$ ) at low field intensity, and approaches the maximum value  $G_{M,\infty}$  at high field intensity when the magnetization saturates, and these two limiting cases can be phenomenologically described by

**Table 4**

Shear storage modulus, MR effect and model parameters of the isotropic and anisotropic CI/SEBS composites obtained from the MDMA measurements.

Sample code	$G_0'$ (MPa)	$G_{M,E}'$ (MPa)	$\Delta G'$ (MPa)	$\Delta G'/G_0'$ (%)	$G_{M,\infty}'$ (MPa)	$a_\psi$ (T <sup>2</sup> )	$R^2$
40CI-SEBS	0.059	0.062	0.003	5	0.062	0.0014	1
40CI-SEBS-300mT	0.060	0.070	0.010	17	0.070	0.0036	0.999
40CI-SEBS-600mT	0.061	0.073	0.012	19	0.073	0.0046	0.999
40CI-SEBS-900mT	0.063	0.080	0.017	27	0.080	0.0048	0.999
40CI-SEBS-1200mT	0.062	0.079	0.017	27	0.079	0.0049	0.999
70CI-SEBS	0.115	0.163	0.048	42	0.162	0.0117	0.997
70CI-SEBS-300mT	0.176	0.296	0.120	68	0.300	0.0078	0.999
70CI-SEBS-600mT	0.204	0.521	0.317	155	0.533	0.0186	0.996
70CI-SEBS-900mT	0.266	0.623	0.357	134	0.637	0.0178	0.996
70CI-SEBS-1200mT	0.263	0.616	0.353	134	0.630	0.0189	0.995

Note:  $G_0'$  is initial storage modulus without external magnetic field.  $G_{M,E}'$  is equilibrium storage modulus under saturated magnetic field.  $\Delta G'$  is the value of  $G_{M,E}'$  subtracting  $G_0'$ , corresponding to the absolute MR effect.  $\Delta G'/G_0'$  is the relative MR effect.  $G_{M,\infty}'$  and  $a_\psi$  are the model parameters estimated from the slopes and the intercepts of the plots of  $\psi^2/G'(\psi)$  versus  $\psi^2$ .

the following equation:

$$\frac{\psi^2}{G_M(\psi)} = \frac{a_\psi}{G_{M,\infty}} + \frac{\psi^2}{G_{M,\infty}} \quad (1)$$

in which  $a_\psi$  is a material parameter [30]. Through the linear relationship of the plots of  $\psi^2/G_M(\psi)$  versus  $\psi^2$ , values of  $G_{M,\infty}$  and  $a_\psi$  can be estimated from the slopes and intercepts. Fig. 7 shows the plots of  $\psi^2/G_M(\psi)$  versus  $\psi^2$  obtained from MDMA measurements (Fig. 6) for the isotropic and anisotropic CI/SEBS composites, and the evaluated parameters of  $G_{M,\infty}'$  and  $a_\psi$  are listed in Table 4. It can be clearly seen from Fig. 7 that the MDMA experimental data of the CI/SEBS composites can be fitted quite well by the phenomenological description in Equation (1) with very good linear relationship when  $\psi$  ranges from 0 to 500 mT, whether the composite is isotropic or anisotropic. It should also be noted from Table 4 that the calculated  $G_{M,\infty}'$  values of the isotropic and anisotropic CI/SEBS composites are very close to the experimental  $G_{M,E}'$  data, nearly the same as the experimental data for 40CI-SEBS composites and 70CI-SEBS composites prepared at low  $\psi_{pre}$ . This phenomenon implies the applicability of Equation (1) for describing the dependence of elastic modulus on the induced magnetic field for these SEBS based MRE materials. Similar to the change of  $G_{M,\infty}'$ ,  $a_\psi$  increases with the increase of  $\phi_{CI}$  and  $\psi_{pre}$  and then reaches a steady value after magnetization saturation. It is evident that both  $G_{M,\infty}'$  and  $a_\psi$  depend on the concentration and distribution of the magnetic particles as well as the strength of the applied magnetic field.

#### 4. Conclusions

CI particles are uniformly and randomly dispersed in the isotropic CI/SEBS composites, while exhibiting ordered chain-like structures along the magnetic field direction in the anisotropic CI/SEBS composite. As for the isotropic composites, the increasing addition of CI particles remarkably improves their thermal stability and mechanical strength without sacrificing their toughness and elasticity, even with high filling of 70wt% CI particles. As for the anisotropic composites, increasing CI concentration and pre-structure temperature, time and magnetic field intensity is beneficial for the formation of more ordered chain-like structures with higher orientation degree and longer particle chains, thus making the smart CI/SEBS composites show more remarkable field induced modulus change and higher MR effect. Moreover, high temperature and long time during pre-structure process have equivalent effect on the magnetorheological property of the CI/SEBS composites, and external magnetic field intensity merely shows obvious influence on the magnetorheological property of the CI/SEBS composites before reaching magnetization saturation.

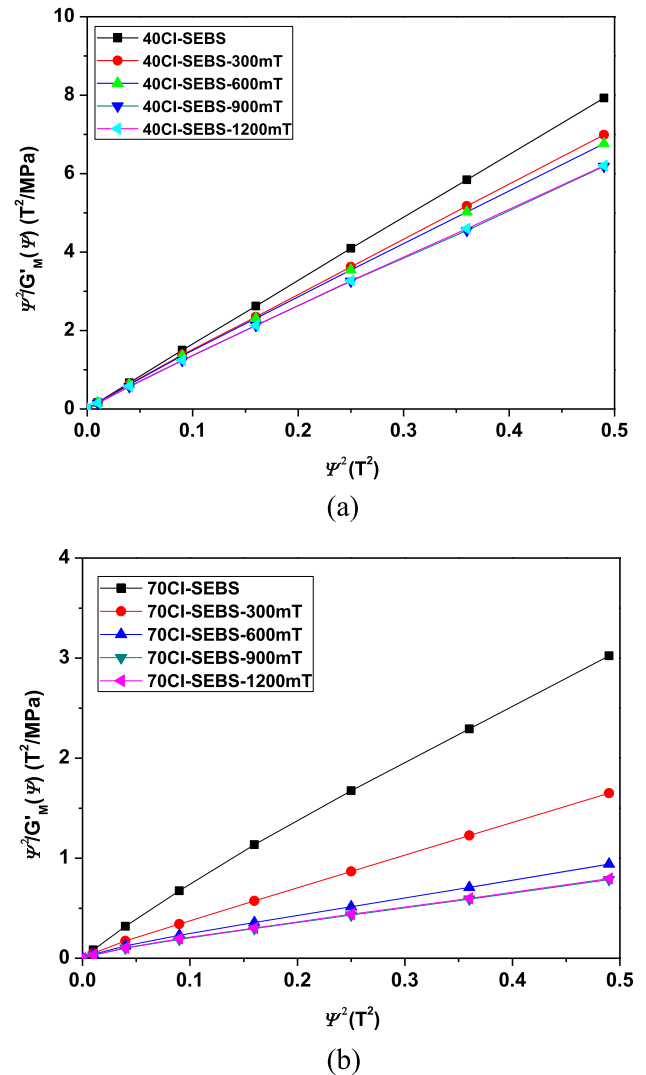


Fig. 7. Plots of  $\psi^2/G'_M(\psi)$  versus  $\psi^2$  obtained from MDMA measurements for the isotropic and anisotropic CI/SEBS composites (a) 40CI-SEBS composites; (b) 70CI-SEBS composites.

#### Acknowledgments

This research was supported by the Science and Technology Research and Development Program from the Ministry of Railways of China (grant No. J2011J002) and Special Science and Technology

Fund for Minhang District - Shanghai Jiao Tong University Cooperation. The authors also thank Instrumental Analysis Center of Shanghai Jiao Tong University for the assistance of the measurements.

## References

- [1] G.Y. Zhou, Q. Wang, Magnetorheological elastomer-based smart sandwich beams with nonconductive skins, *Smart Mater. Struct.* 14 (2005) 1001–1009.
- [2] N. Kchit, G. Bossis, Electrical resistivity mechanism in magnetorheological elastomer, *J. Phys. D. Appl. Phys.* 42 (2009) 105505.
- [3] L.J. Mietta, G. Jorge, R.M. Negri, A flexible strain gauge exhibiting reversible piezoresistivity based on an anisotropic magnetorheological polymer, *Smart Mater. Struct.* 23 (2014) 085026.
- [4] N. Kchit, P. Lancon, G. Bossis, Thermo-resistance and giant magnetoresistance of magnetorheological elastomers, *J. Phys. D. Appl. Phys.* 42 (2009) 105506.
- [5] X.C. Guan, X.F. Dong, J.P. Ou, Magnetostrictive effect of magnetorheological elastomer, *J. Magn. Magn. Mater.* 320 (2008) 158–163.
- [6] B.X. Ju, M. Yu, J. Fu, Q. Yang, X.Q. Liu, X. Zheng, A novel porous magnetorheological elastomer: preparation and evaluation, *Smart Mater. Struct.* 21 (2012) 035001.
- [7] S. Sun, H.X. Deng, J. Yang, W.H. Li, H.P. Du, G. Alici, M. Nakano, An adaptive tuned vibration absorber based on multilayered MR elastomers, *Smart Mater. Struct.* 24 (2015) 045045.
- [8] N. Hoang, N. Zhang, H. Du, An adaptive tunable vibration absorber using a new magnetorheological elastomer for vehicular powertrain transient vibration reduction, *Smart Mater. Struct.* 20 (2011) 015019.
- [9] L. Chen, X.L. Gong, W.Q. Jiang, J.J. Yao, H.X. Deng, W.H. Li, Investigation on magnetorheological elastomers based on natural rubber, *J. Mater. Sci.* 42 (2007) 5483–5489.
- [10] J.K. Wu, X.L. Gong, L. Chen, H.S. Xia, Z.G. Hu, Preparation and characterization of isotropic polyurethane magnetorheological elastomer through in situ polymerization, *J. Appl. Polym. Sci.* 114 (2009) 901–910.
- [11] B.X. Ju, R. Tang, D.Y. Zhang, B.L. Yang, M. Yu, C.R. Liao, Temperature-dependent dynamic mechanical properties of magnetorheological elastomers under magnetic field, *J. Magn. Magn. Mater.* 374 (2015) 283–288.
- [12] B. Wei, X.L. Gong, W.Q. Jiang, Influence of polyurethane properties on mechanical performances of magnetorheological elastomers, *J. Appl. Polym. Sci.* 116 (2010) 771–778.
- [13] Y.L. Wang, Y. Hu, Y.L. Wang, H.X. Deng, X.L. Gong, P.Q. Zhang, W.Q. Jiang, Z.Y. Chen, Magnetorheological elastomers based on isobutylene isoprene rubber, *Polym. Eng. Sci.* 46 (2006) 264–268.
- [14] T.L. Sun, X.L. Gong, W.Q. Jiang, J.F. Li, Z.B. Xu, W.H. Li, Study on the damping properties of magnetorheological elastomers based on cis-polybutadiene rubber, *Polym. Test.* 27 (2008) 520–526.
- [15] Y. Hu, Y.L. Wang, X.L. Gong, X.Q. Gong, X.Y. Zhang, W.Q. Jiang, P.Q. Zhang, Z.Y. Chen, New magnetorheological elastomers based on polyurethane/Si-rubber hybrid, *Polym. Test.* 24 (2005) 324–329.
- [16] P. Blom, L. Kari, Amplitude and frequency dependence of magneto-sensitive rubber in a wide frequency range, *Polym. Test.* 24 (2005) 656–662.
- [17] P. Zajac, J. Kaleta, D. Lewandowski, A. Gasperowicz, Isotropic magnetorheological elastomers with thermoplastic matrices: structure, damping properties and testing, *Smart Mater. Struct.* 19 (2010) 045014.
- [18] H. Bose, R. Roder, Magnetorheological elastomers with high variability of their mechanical properties, *J. Phys. Conf. Ser.* 149 (2009) 012090.
- [19] G.V. Stepanov, S.S. Abramchuk, D.A. Grishin, L.V. Nikitin, E.Y. Kramarenko, A.R. Khokhlov, Effect of a homogeneous magnetic field on the viscoelastic behavior of magnetic elastomers, *Polymer* 48 (2007) 488–495.
- [20] H.J. Song, N.M. Wereley, R.C. Bell, J.L. Planinsek, J.A. Filer, Field dependent response of magnetorheological elastomers utilizing Fe spherical particles versus Fe nanowires, *J. Phys. Conf. Ser.* 149 (2009) 012097.
- [21] S. Aloui, M. Kluppel, Magneto-rheological response of elastomer composites with hybrid-magnetic fillers, *Smart Mater. Struct.* 24 (2015) 025016.
- [22] H. Bose, Viscoelastic properties of silicone-based magnetorheological elastomers, *Int. J. Mod. Phys. B* 21 (2007) 4790–4797.
- [23] W. Zhang, X.L. Gong, J.F. Li, H. Zhu, W.Q. Jiang, Radiation vulcanization of magnetorheological elastomers based on silicone rubber, *Chin. J. Chem. Phys.* 22 (2009) 535–540.
- [24] Y.C. Fan, X.L. Gong, W.Q. Jiang, W. Zhang, B. Wei, W.H. Li, Effect of maleic anhydride on the damping property of magnetorheological elastomers, *Smart Mater. Struct.* 19 (2010) 055015.
- [25] J.F. Li, X.L. Gong, H. Zhu, W.Q. Jiang, Influence of particle coating on dynamic mechanical behaviors of magnetorheological elastomers, *Polym. Test.* 28 (2009) 331–337.
- [26] M. Behrooz, J. Sutrisno, L.Y. Zhang, A. Fuchs, F. Gordaninejad, Behavior of magnetorheological elastomers with coated particles, *Smart Mater. Struct.* 24 (2015) 035026.
- [27] X.Y. Qiao, X.S. Lu, W.H. Li, J. Chen, X.L. Gong, T. Yang, W. Li, K. Sun, X.D. Chen, Microstructure and magnetorheological properties of the thermoplastic magnetorheological elastomer composites containing modified carbonyl iron particles and poly(styrene-*b*-ethylene-ethylene-propylene-*b*-styrene) matrix, *Smart Mater. Struct.* 21 (2012) 115028.
- [28] H.M. Tiggemann, D. Tomachesdi, F. Celso, V.F. Ribeiro, S.M.B. Nachtigall, Use of wollastonite in a thermoplastic elastomer composition, *Polym. Test.* 32 (2013) 1373–1378.
- [29] L. Chen, X.L. Gong, W.H. Li, Effect of carbon black on the mechanical performances of magnetorheological elastomers, *Polym. Test.* 27 (2008) 340–345.
- [30] J.K. Wu, X.L. Gong, Y.C. Fan, H.S. Xia, Improving the magnetorheological properties of polyurethane magnetorheological elastomer through plasticization, *J. Appl. Polym. Sci.* 123 (2012) 2476–2484.